# Chapter 3
# Femtosecond Mode-Locked Semiconductor Disk Lasers

**Uwe Griebner, Peter Klopp, Martin Zorn and Markus Weyers**

**Abstract** The generation of ultrashort pulses with passively mode-locked semiconductor disk lasers (SDLs) incorporating only an optically-pumped surface-emitting semiconductor gain element and a semiconductor saturable absorber mirror (SESAM) is presented. The optimum parameters for nearly Fourier-limited femtosecond pulses in single- or multiple-pulse regimes are investigated. On the basis of the experience gained a harmonically mode-locked SDL emitting sub-200 fs pulses at a very high repetition rate of 92 GHz and a fundamentally mode-locked SDL generating practically chirpfree pulses with durations close to 100 fs at a rate of 5 GHz are demonstrated in the 1-μm wavelength range. The latter set a record for shortest pulse durations achieved directly from any fundamentally or harmonically mode-locked semiconductor laser. Overall, the results are a further step of modelocked SDLs in becoming useful compact and low-cost ultrashort-pulse sources.

## 3.1 Introduction

Semiconductor disk lasers (SDLs), also called optically-pumped vertical-external-cavity surface-emitting lasers (VECSELs) or optically pumped semiconductor lasers (OPSLs), are a relatively new laser family combining high output power,

U. Griebner (✉) · P. Klopp
Max-Born-Institut für Nichtlineare Optik und Kurzzeitspektroskopie,
Max-Born-Straße 2 A, 12489 Berlin, Germany
e-mail: griebner@mbi-berlin.de

*Present Address:*
M. Zorn
JENOPTIK Diode Lab GmbH, Berlin, Germany

M. Weyers · M. Zorn
Ferdinand-Braun-Institut, Leibniz-Institut für Höchstfrequenztechnik,
Gustav-Kirchhoff-Str. 4, 12489 Berlin, Germany



S. Nolte et al. (eds.), *Ultrashort Pulse Laser Technology*,
Springer Series in Optical Sciences 195, DOI 10.1007/978-3-319-17659-8_3

wide wavelength coverage, and high beam quality. Another attractive feature of the SDL concept is the potential of ultrashort-pulse generation at high repetition rates, which is the focus of this chapter.

In general, semiconductor heterostructures enable compact and cheap lasers operating in continuous-wave (cw) or pulsed regimes. Semiconductor bandgap engineering gives large freedom concerning the emission wavelength, which can be chosen almost anywhere from ≈340 nm to ≈30 μm [1, 2]. Femtosecond mode-locked semiconductor disk lasers have the potential to replace rather complex, expensive laser systems and to establish ultrashort-pulse applications outside of scientific laboratories. Furthermore, the typically high pulse repetition rates of ≥1 GHz make SDLs attractive, e.g., for THz time-domain spectroscopy with asynchronous optical sampling (ASOPS) [3] or for frequency comb generation [4]. The high pulse repetition rates of mode-locked SDLs are also interesting for communication applications [5].

Compared to edge-emitting semiconductor lasers [6], in vertical-cavity surface-emitting lasers (VCSELs) [7] the laser cavity axis and the light emission are perpendicular to the plane of the epitaxial laser structure, allowing the emission of a circular fundamental transverse-mode beam. However, increasing the output beam diameter to larger than 10 μm, the laser output becomes multimode, and uniform current injection over such large areas is difficult with edge injection through transparent contact layers. A solution to realize carrier excitation uniformly across such a large area is optical pumping. Efficient and simple continuous-wave semiconductor diode lasers with multi-mode emission and high output power levels can be used as pump sources.

The laser concept of optically pumped vertical-external-cavity surface-emitting lasers (VECSELs) or semiconductor disk lasers (SDLs) was developed about one decade ago [8]. An SDL pumped by a multimode laser diode can be considered as a diode-pumped solid-state laser, where the gain medium consists of a semiconductor structure instead of a classical ion-doped crystal or glass. The laser geometry resembles the well-established solid-state disk laser configuration [9], where a thin solid-state gain medium, such as an Yb-doped crystal, with a high-reflecting dielectric backside coating is used as an active mirror and placed directly on a heat sink. In the simplest SDL design, an additional spherical mirror and a highly reflective mirror (usually a Bragg mirror consisting of semiconductor layers with different refractive indices) underneath the semiconductor gain medium (usually a multi-quantum-well structure) constitute the laser cavity. Using SDLs, cw output powers of several 10 W have been demonstrated with excellent beam quality [10, 11].

Similar to diode-pumped solid-state lasers, SDLs can be passively mode-locked by introducing a semiconductor saturable absorber mirror (SESAM) into the cavity [5]. However, there is a great difference between dielectric gain materials such as ion-doped crystals or glass and semiconductor gain media. The latter exhibit several

orders of magnitude larger absorption and emission cross sections, resulting in low gain saturation fluences and short upper-state lifetimes. This limits the amount of stored energy in the gain material and the minimum achievable pulse repetition rates. Due to low saturation fluences, Q-switched mode-locking instabilities are strongly reduced [12], which is an important advantage for achieving very high pulse repetition rates. The full potential of semiconductor lasers for ultrashort-pulse generation has not yet been exploited. In principle, the gain bandwidth of semiconductor lasers allows fundamental or harmonic mode-locking with sub-100-fs pulse durations [13].

For a long time it was believed that the pulse durations now achieved by mode-locked SDLs could be obtained only from oscillators using dielectric or dye media and not from semiconductor lasers, since the strong carrier-density dependence of the complex refractive index and the carrier dynamics in semiconductors introduce a strong chirp. One of the first passively mode-locked SDLs, demonstrated in 2000 by Hoogland et al., generated 22-ps pulses at a repetition rate of 4 GHz [14]. Since that time, considerable progress has been made in terms of spectral coverage, output power, pulse duration, and repetition rate [5]. Experiments with SESAM-mode-locked SDLs showed that in some operation regimes the chirp contributions approximately compensate each other. In this case, one may obtain something like a "soliton-like" pulse [15]. Nevertheless, the minimum achievable pulse duration in this case had not been much shorter than about half a picosecond [16, 17]. From monolithic edge-emitting lasers, there were demonstrations of sub-500 fs pulses. Such a laser was reported to reach a repetition rate of >1 THz with a pulse width of 260 fs [18], but in this case one had to speak rather of a sine-shaped output instead of separate pulses. While the asymmetric beam profile is a general difficulty with edge-emitting semiconductor lasers, additional problems connected with pulse shortening are the large amounts of dispersion and nonlinearities introduced due to the long interaction length. As a result, strongly chirped pulses and increased timing jitter can occur. As an example, 395-fs pulses at 21 GHz with a time-bandwidth product of ≈1 were achieved from a monolithic two-section quantum dot laser which is about three times larger than the Fourier limit [19].

In 2008, we demonstrated a practically chirp-free 290-fs SDL [20] and Wilcox et al. showed 260-fs pulses from a similar laser [21]. After these milestones, we were able to further reduce the emitted pulse duration of mode-locked SDLs to 190 fs at 3 GHz pulse repetition rate [22] and then to 107 fs at 5 GHz [23]. Furthermore, we observed extraordinarily high pulse repetition rates from an SDL. In [24], Lorenser et al. reported a rate of 50 GHz, obtained with a pulse duration of ≈3 ps. We improved this value to ≈92 GHz with sub-200-fs pulses.

In this chapter, we present design criteria and experimental conditions for ultrashort-pulse generation from mode-locked SDLs with an emission wavelength

around 1 μm. We describe different regimes of laser operation and present almost transform-limited pulses at very high repetition rates or with a shortest duration in the 100-fs range.

## 3.2 Semiconductor Elements

### *3.2.1 Design, Growth, and Processing*

For the semiconductor elements of a sub-picosecond SDL, there are specific requirements which follow from the pulse shaping process and determine our design strategy. As we will show in the following paragraphs, pulse shaping in such SDLs cannot be described with the "soliton-like mode-locking" picture applicable to ultrashort-pulse lasers with dielectric gain media or to picosecond SDLs [25]. Instead, we found fast and suitably strong amplitude modulation, in particular, a fast saturable absorber, spectral matching of the elements, and minimized group delay dispersion (GDD) to be key issues. Furthermore, a larger gain bandwidth is expected to support shorter pulses, too. The SESAMs and the SDL gain structures studied were designed for laser operation with a center wavelength around 1030 nm. The design was assisted by simulation, mainly with respect to GDD.

All epitaxial layers were grown by metalorganic vapor phase epitaxy (MOVPE) in an Aixtron 200/4 reactor in 3 × 2″ configuration. The sources used were trimethylgallium, trimethylaluminum, trimethylindium, arsine, and phosphine. For the SDL gain elements, removal of the heat from the optically pumped region is crucial. GaAs has a relatively low thermal conductivity and thus the substrate hinders the heat dissipation. Transparent heat sinks like diamond on the surface of the gain chip are technologically challenging (bonding is difficult) and affect dispersion. Therefore, we used gain structures where the Bragg mirror was attached directly to a heat sink and the substrate was removed. This made it necessary to first grow the active periodic gain structure with the quantum wells (QWs) and then the Bragg mirror. The active part was grown at 650 °C and the distributed Bragg reflector (DBR mirror) at 700 °C. The wafer was cut into 2 × 2 $mm^2$ or 4 × 6 $mm^2$ pieces, which were mounted mirror-side down ("bottom up") on CuW heat sinks of the same size using AuSn solder. Afterwards the substrate was etched off with an aqueous solution of sulphuric acid and hydrogen peroxide. A ≈300-nm-thick $In_{0.48}Ga_{0.52}P$ layer served as an etch-stopper. Finally, an antireflective dielectric coating was applied and the soldered structure was mounted onto a large copper heat sink.

For the SESAM structure the DBR mirror was grown at 770 °C, while the InGaAs QW was grown at 510 °C. After coating the wafer backside with metal, the SESAM wafers were diced and the chips were soldered onto a CuW submount [26]. These submounts were attached to a Peltier cooling/heating element that allowed for a variation of the band edge via changing the temperature.

### 3.2.2 Semiconductor Saturable Absorber Mirror

Our SESAM structures for the 1 μm wavelength range consisted of a single InGaAs QW sandwiched between two GaAs layers grown on an AlAs/(Al)GaAs DBR mirror. The indium content in the QW defined the operation wavelength [27]. Usually a $SiN_x$ (or comparable) antireflection coating was applied. This also provided a protection of the GaAs surface against oxidation. To achieve very short carrier recombination times in the QW and by this a fast over-all recovery of the absorber, two approaches were studied. First, the QW was surrounded by equally thick (approximately 60–70 nm) GaAs layers. As-clusters and point defects were created in the QW by implanting arsenic (As) ions. Subsequent annealing results in the formation of As clusters in the InGaAs QW, enhancing recombination [28, 29]. The second type of SESAM structure employed a "surface-near" QW without implantation to achieve short relaxation times via surface states. "Surface-near" means that the upper GaAs layer was only a thin cap, whose thickness was varied between 1 and 5 nm. Such a "surface-near" SESAM structure is shown in Fig. 3.1a. In general, the surface-near QWs showed a shorter relaxation time compared to the ion treated ones. For the $SiN_x$ coating two different thicknesses were tested, resulting in a non-resonant and a resonant design. Best results with respect to short pulse durations were obtained using the non-resonant design.

The resonant responses of surface-near SESAMs were characterized by pump-probe and nonlinear reflectivity measurements. For this purpose, the emission of a mode-locked Yb-laser delivering pulses with a duration of ≈250 fs at 1030 nm (*Amplitude*, model: *MIKAN*) was focused on the sample. This SESAM had a 2-nm GaAs cap layer and was the absorber device operating in the SDL with the shortest pulse duration (paragraph 5).

Pump-probe traces are shown in Fig. 3.2a for two values of the pulse fluence. In general, with a pump and probe pulse duration of a few hundred fs at low to moderate fluences, a measured SESAM response (change of reflectivity versus

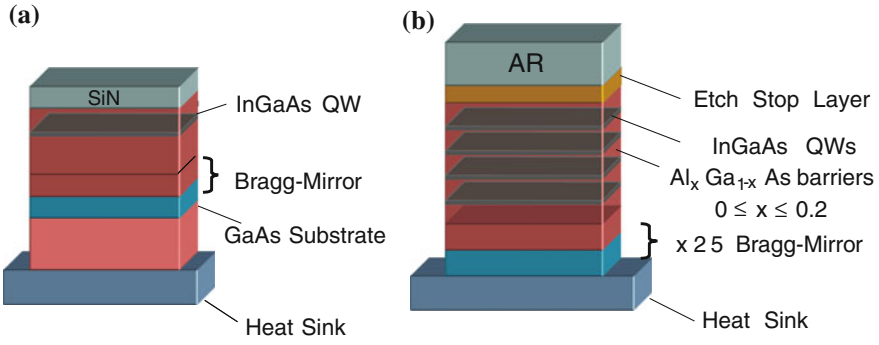


**Fig. 3.1** Structure of the semiconductor elements: **a** "Surface-near" semiconductor saturable absorber mirror (SESAM). **b** Surface-emitting 4-QW gain structure

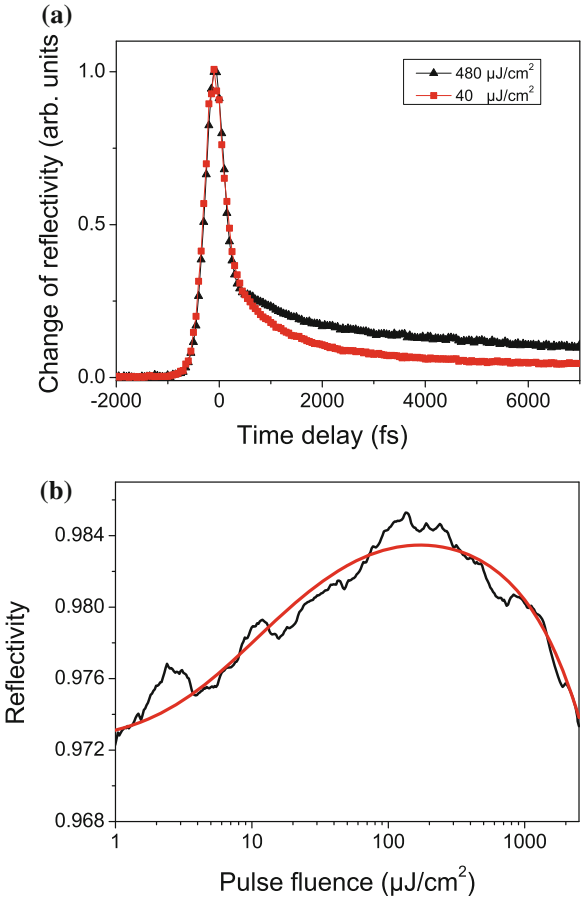


**Fig. 3.2** Pump-probe response (**a**) and nonlinear reflectivity (**b**) of the surface-near QW semiconductor saturable absorber mirror. The *red curve* in (**b**) is a fit of the saturation behavior including two-photon absorption

pump-probe delay) consists of different parts. The "fast component" exhibits a decay time in the order of the pulse duration (here: <300 fs) and is related to spectral hole-burning (SHB). SHB means carriers that have been excited by a pump pulse with a limited spectral bandwidth will first occupy only states within a certain range of energies in the conduction band and will therefore lead to a spectrally selective bleaching of absorption (Pauli blocking). This bleaching will relax when the carrier distribution broadens by carrier-carrier and carrier-phonon scattering, resulting in a weaker bleaching of the whole band. The effect of carrier-carrier scattering is visible in the fast component. There may also be a fast contribution by exciton ionisation, depending on the relative energies of excitation phonons and of the heavy-hole exciton resonance. However, in our surface-near SESAMs at room temperature and above, the exciton resonance can be assumed to be smeared out strongly. The "slow component" is contributed by carrier-carrier scattering and interband relaxation, i.e., carrier recombination, with the latter more or less dominating. Spatial diffusion time of the free carriers will also play a role, if there are no recombination centers nearby.

In Fig. 3.2a, in case of the lower value of the pulse fluence (40 μJ/cm$^2$), the total 1/*e* absorber relaxation time was about 1 ps. This indicates an enhanced tunneling of carriers into surface states. Since these states lie between conduction and valence band in terms of energy, their presence, unaffected by the additional SiN layer, greatly accelerates the interband relaxation process. A comparison of pump-probe response measurements at 1060 nm between SESAMs with an As-ion-treated or a surface-near QW (2-nm cap) can be found in [30]. As-ion implantation yielded longer 1/*e* relaxation times (3 ps and more compared to 1 ps). Thicker GaAs caps (>2 nm), too, resulted in significantly slower recombination. All experiments presented in the following paragraphs were performed using SESAMs with a near-surface QW and a 2-nm GaAs cap. So far, we have not been able to generate any femtosecond pulses with slower types of absorbers.

When the pulse fluence in Fig. 3.2a was increased from 40 to 480 μJ/cm$^2$, the shape of the absorber response changed and the absorption recovered more slowly, with a 1/*e* relaxation time of >2 ps. This can be explained by a stronger saturation of the fast, SHB-related component compared to the slower one. The observation does not support the hypothesis of an optical Stark effect in the SESAM as the dominant pulse shaping mechanism in sub-picosecond SDLs, which had been proposed by Wilcox et al. [21]. This would predict a faster response for higher fluences. A more detailed discussion of this issue is included in [22].

The observed SESAM behavior has important consequences for mode-locked SDLs, which have to rely on a fast absorber for ultrashort-pulse generation: The shorter the pulse duration in the SDL cavity, the more important the fast component of the absorber response. Hence, SHB helps to shape ultrashort pulses. The higher the pulse fluence, the slower the overall relaxation of the SESAM. For shorter pulses, oversaturation of the absorber will more strongly affect the pulse shaping. Hence, SHB makes it more difficult to stabilize the mode-locking regime. The complex temporal absorption behavior also corresponds to other pulse-shaping effects, i.e., spectral dynamics (dynamic filtering) and self phase modulation (SPM). Please note that the semiconductor gain element will show, to some degree, analogue behavior (SHB in the gain spectrum, fast and slow gain relaxation components, stronger gain saturation for shorter pulses, gain filter dynamics, SPM).

The nonlinear reflectivity of the surface-near SESAM was measured with the laser mentioned above at 1030 nm in a setup similar to the one reported in [31]. The SESAM was heated to a temperature of 68 °C, which corresponded to the operating point in the SDL laser experiment delivering the shortest pulses of 107 fs at 1030 nm. The measured absolute reflection of the SESAM versus input pulse fluence is depicted in Fig. 3.2b. We extract a saturation fluence of about 10 μJ/cm$^2$, a modulation depth of ≈1.2 %, and a nonsaturable loss of ≈1.5 %. With increasing pulse fluence (>100 μJ/cm$^2$), two-photon absorption can be observed, leading to a decrease of the reflectivity and, in the worst case, to damage of the device. Additional nonlinear reflectivity measurements were performed for SESAM temperatures of 46 and 22 °C, delivering modulation depths of ≈0.8 and ≈0.6 %, respectively. The reduced modulation depth is related to the corresponding shift of exciton resonance and band gap to higher energies. This behavior is schematically illustrated in Fig. 3.7, cf. Sect. 3.4.1.

### 3.2.3 SDL Gain Structure

A simplified surface-emitting SDL gain structure is shown in Fig. 3.1b. Similar to the SESAM structures, the SDL gain chips consisted of an AlAs/GaAs DBR mirror followed by an active region. The active section contained InGaAs QWs and (Al)GaAs barriers. SDL gain structures were tested with different barriers and QW numbers (3–13 QWs). We investigated two different barrier configurations: The simpler one used GaAs barriers and is denoted in the following as step-index structure (STIN, see [32] and Fig. 3.3a). The second barrier design used graded $Al_xGa_{1-x}As$ layers having an aluminum content of x = 0 at the QW side and of x = 0.2 at the AlGaAsP strain compensation layer (graded-index or GRIN structure, see also [32] and Fig. 3.3b). The AlGaAsP strain compensating layers (not contained in the simplified design in Fig. 3.1b) had to be introduced since the high strain incorporated by the InGaAs QWs would otherwise cause lattice relaxation

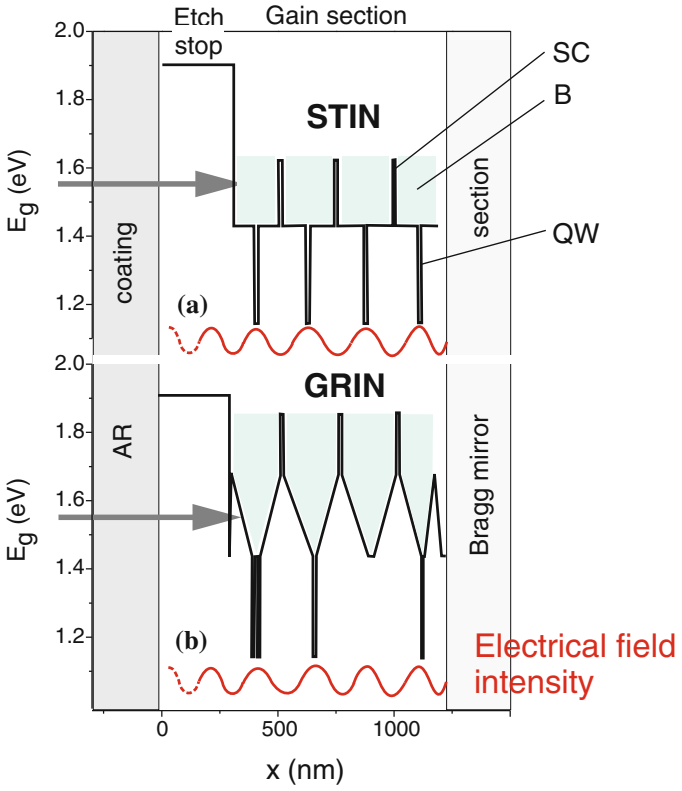


**Fig. 3.3** Schematic band gap diagrams of 4-quantum well (QW) gain structures with step index (STIN) (**a**) and graded index (GRIN) design (**b**). *Arrows* mark the excitation photon energy (*SC* strain compensation, *B* barriers)

and formation of dislocation networks. Such would reduce the radiative recombination and can lead to rapid device degradation.

Figure 3.3 schematically shows the band gap diagram of the GRIN gain structure in comparison to a step index (STIN) architecture. The QWs were placed into the electric-field maxima of the interference pattern formed by the incident and reflected light beam (see red curves in Fig. 3.3), thus increasing the longitudinal confinement and consequently the gain. We varied the numbers of QWs in the antinodes of the electrical field. For example, by introduction of a double quantum well and omitting the last but one QW in our structure, the amount of pump power provided to each QW was modified (Fig. 3.3b). In our case, this meant unequal pumping of the QWs and resulted in an inhomogeneous broadening of the gain spectrum of the structure, supporting shorter pulses. The pump radiation is mainly absorbed by the spacer layers, and subsequently the generated carriers drift into the QWs. A graded Al-content of the barriers results in a graded bandgap and thereby in a quasi-electric field, which promotes the carrier drift towards the QWs. This was confirmed by time-resolved photo luminescence (PL) experiments. The rise time of the QW PL after barrier excitation was determined to be 17.7 ps for the STIN gain section, whereas the corresponding value observed for the GRIN gain section was <5 ps [32]. Because of the superior carrier collection capability, the GRIN design, which we used for most of our gain media, is expected to result in higher laser efficiency compared to the STIN-design [32].

Figure 3.4 shows the reflectance measurement of an SDL gain structure before the antireflection (AR) coating. The reflectance was measured using a tungsten white-light source. A reflectance stop band centered around 1030 nm was observed, since the element was designed to serve as a mirror of the laser cavity. Due to the missing AR coating, a resonance was formed within the gain structure, resulting in the deep reflectance decrease at 1026 nm. The corresponding PL measurement, performed with a semiconductor laser diode exciting at 797 nm, is also shown in Fig. 3.4. Comparing the spectra measured with and without AR coating, the influence of the cavity resonance effect is clearly visible. Without AR coating the peak was shifted towards the resonance wavelength and a second small peak appeared at 970 nm near the stop band edge. Only after AR coating, the undisturbed PL emission was measured, since the resonance had practically disappeared due to the minimized reflectance at the SDL/air interface. The undisturbed PL exhibited a FWHM of about 20 nm, indicating that the gain medium should principally allow laser pulse durations in the sub-100-fs range.

We obtained sub-ps laser pulses only with AR-coated SDL gain chips. The AR coating has a strong influence on the group delay dispersion (GDD) of the gain element as shown in Fig. 3.5, where an uncoated and a coated GRIN structure are compared. In the uncoated case, the element showed the spectral-phase characteristics of a Gires-Tournois interferometer (GTI). For femtosecond SDLs, the structure thickness and hence the spectral positions of the GTI resonances are chosen such that the GTI is operated in the vicinity of zero dispersion [16]. However, these positions depend on the operation temperature (Fig. 3.5). Furthermore, the dispersion varies considerably over the spectral width of a short pulse, and there are

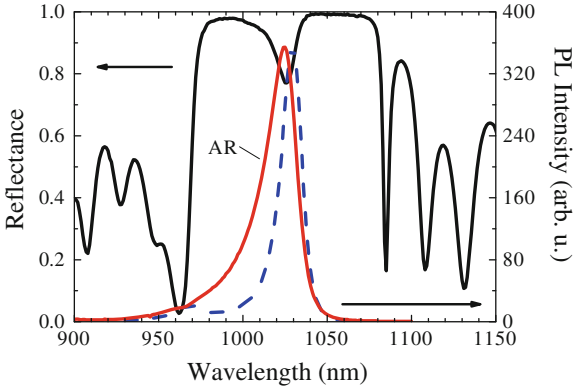


**Fig. 3.4** Measured reflectance (*left axis*) and photoluminescence (*right axis*) of an SDL gain structure (STIN design with 6 QWs). The photoluminescence was additionally measured after the antireflection coating (*dashed line*)

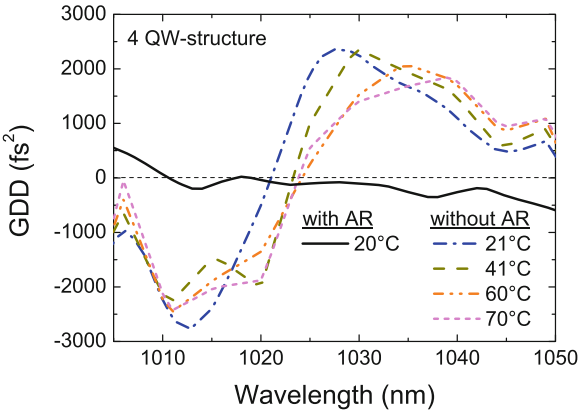


**Fig. 3.5** Group delay dispersion (GDD) of a 4-QW GRIN gain structure. An AR-coated sample (*black solid line*) is compared with an uncoated sample made from the same wafer. The latter shows a significant temperature dependence as indicated by the *other curves*

also dispersion dynamics due to the interplay of GTI resonance and the gain or absorption spectrum changed by the pulse. With AR coating, the measured dispersion is low for all wavelengths, i.e., always below the resolution limit (≈±200 fs$^2$) of our white-light interferometer (black solid line in Fig. 3.5). Nevertheless, we can expect a thin structure with 3 or 4 QWs to have lower residual dispersion compared to a thicker one with, e.g., 6 or 13 QWs, since the GDD is proportional to the square of the thickness of the structure [33]. This motivated the development of three- and four-QW gain media for shortest pulse operation. The above mentioned findings are also valid for the SESAM structures used here, but to a lesser degree, because their active zone is very thin (one QW only).

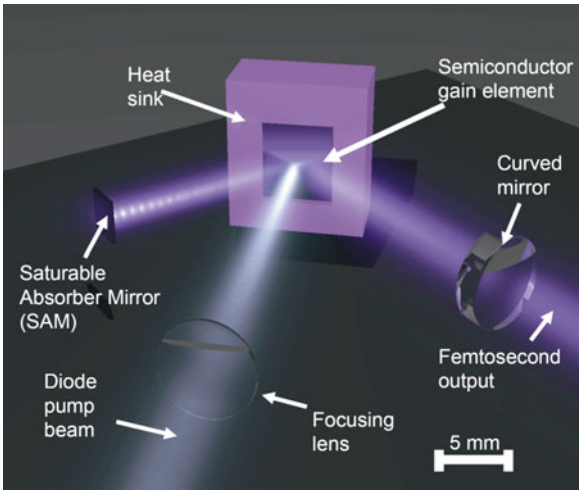


**Fig. 3.6** Setup of a mode-locked semiconductor disk laser (SDL). The *V-shaped* cavity contains a saturable absorber mirror (SESAM) as the mode-locker, an InGaAs/AlGaAs disk gain element at the folding point, and a curved output coupler

## 3.3 Setup of the Mode-Locked Semiconductor Disk Laser

Figure 3.6 shows the scheme of a V-folded, nearly hemispherical SDL oscillator consisting of only three elements: the SDL gain structure, the SESAM and the curved output coupler. The temperature of both semiconductor elements can be independently controlled by the Peltier elements on which they are mounted. The length of the resonator was typically around 50 mm. There was a tight focus with a waist size of roughly 15–20 μm to create a high pulse fluence (several times the saturation fluence) on the SESAM. An estimation of the focus size is difficult, since solder-related deformations of the gain chip (see [26]) and a deviation of the output coupler curvature from its nominal value prevent an exact calculation. Our SDLs were optically pumped by diode lasers emitting around 800 or 840 nm.

## 3.4 Parameters for the Generation of Femtosecond Pulses from Mode-Locked Semiconductor Disk Lasers

### *3.4.1 Spectral Tuning of the SESAM*

The subject of paragraph 4 is the influence of adjustable laser parameters on the ultrashort-pulse performance. At first, we investigated the relative energetic settings of the laser photon energy and of the SESAM band edge and exciton resonance.

For our initial experiments, we chose a 6-QW STIN gain chip and three different SESAMs, whose room temperature photoluminescence varied from one to the other by steps of 10 nm. With one of the absorbers, stable mode-locking with sub-ps pulse durations was achieved. The result is listed in Table 3.1 as experiment no. 1.

**Table 3.1** Optimum SESAM temperatures for shortest-pulse generation from our SDLs

| Experiment no. | SESAM PL at (nm) | SESAM temperature (°C) | Exciton transition at (nm) | Gain chip | Laser emission at (nm) | Minimum pulse duration (fs) | Comment/ Reference |
|---|---|---|---|---|---|---|---|
| 1 | 1028 | 43 | **1025** | A 6 QW | **1040** | 590 | [27] |
| 2 | 1028 | 59 | **1030** | B 4 QW | **1033** | 350 | [34] |
| 3 | 1031 | 61 | **1033** | C 4 QW | **1036** | 290 | [20] |
| 4 | 1031 | 85 | **1040** | C 4 QW | **1039** | 300 | Figure 3.9 |
| 5 | 1031 | 106 | **1047** | D 4 QW | **1045** | 210 | Figures 3.10, 3.11 and 3.12 |
| 6 | 1031 | 111 | **1048** | D 4 QW | **1044** | 190 | [22] |
| 7 | 1050 | 54 | **1050** | D 4 QW | **1045** | 210 | – |
| 8 | 1028 | 20 | **1018** | E 4 QW | **1021.5** | 198 | Figure 3.13 |
| 9 | 1028 | 68 | **1032** | F 3 QW | **1030** | 107 | Figure 3.14 |

Three near-surface SESAMs (photoluminescence at 1028, 1031, 1050 nm) and six gain chips (*A*–*F*) were used. *Bold numbers* The wavelength of the SESAM exciton transition (error ±5 nm) is compared to the respective laser emission wavelength

Using the setup of Fig. 3.6 with a 0.5 % transmission output coupler, practically chirp-free pulses as short as 590 fs were generated with an average output power of 30 mW at 1040 nm [27]. For this absorber, we found that the SESAM exciton energy was slightly higher than the energy of the laser photons. Figure 3.7a illustrates this situation, where the laser is operated on the red side of the exciton resonance of the SESAM.

A way to determine the position of the exciton resonance is from a photocurrent (PC) spectrum of the SESAM, which was recorded using a Fourier-transform spectrometer. The position is approximately at the maximum of $dI_{PC}/dE$ (see Fig. 3.7b; $I_{PC}$, photocurrent; $E$, excitation photon energy). The PL maximum of the above absorber was at 1028 nm, while the PC measurement yielded an exciton transition wavelength of 1015 nm. From further comparisons of PL spectra with PC spectra, we assume that for our type of SESAM at room temperature the heavy-hole exciton resonance is generally ≈10 nm below the PL maximum [27]. We found a variation of this shift in the range of ±5 nm, which we attribute basically to the difficulties in determining the exciton position in the PC spectrum. Band gap and exciton resonance are no sharp features, but smeared towards lower and higher energies by temperature-related and structurally induced broadening. While a sharp exciton transition should cause a significant dependence of the dynamic behavior on the excitation energy or on the absorber temperature, we did not find clear signs

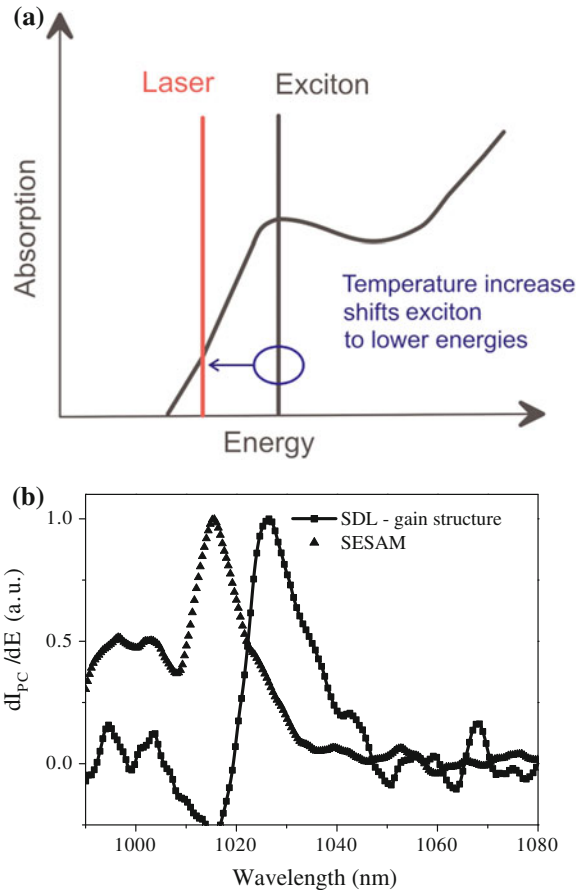


**Fig. 3.7** Scheme of the energetic position of the SESAM exciton resonance (marked by *black vertical line*) relative to the laser photon energy (*red marker*). The *arrow* symbolizes that exciton resonance and band edge can be shifted by temperature tuning (**a**). Photocurrent measurements of SDL gain structure and SESAM at room temperature (**b**)

of this in pump-probe measurements of our SESAMs. Therefore, the exciton transition is to be understood mainly as a landmark to characterize the operating point on the slope of the SESAM absorption spectrum. This operating point will determine the modulation depth of the SESAM and the dynamic spectral filtering effect, which both strongly affect the mode-locked laser regime. In the above experiment, taking into account the SESAM temperature (43 °C), the laser wavelength was roughly 15 nm above the exciton transition. From the nonlinear-reflectivity measurements of this absorber in paragraph 2.2., we estimate ≈0.5 % of saturable absorption for this case.

For our next experiment (labeled no. 4 in Table 3.1), we used a similar SESAM with a PL maximum at 1031 nm. By heating of the SESAM, the exciton resonance and the band gap of the device were tuned towards the laser photon energy (see arrow in Fig. 3.7a). This increased the effective saturable absorption, providing stronger pulse shaping. Compared to the initial experiments, we reduced the number of QWs in the gain structure to minimize the dispersion; we chose a 4-QW GRIN structure

containing two single QWs and a double QW as shown in Fig. 3.3b). The heat sink temperature of the gain chip was kept at 19 °C. The optical pump power at 840 nm amounted to 0.92 W, and an 0.5 % output coupler was used. The SESAM temperature was increased from room temperature to 93 °C. At room temperature, the laser photon energy was far below the energies of the band gap and the heavy-hole exciton resonance of the absorber. By heating of the SESAM, these spectroscopic features were red-shifted towards the laser photon energy by 0.25 meV/°C (0.3 nm/°C). Absorption increased from practically zero for the SESAM at room temperature, which resulted in an output power of 21 mW, to values in the order of 1 %, indicated by the considerable decrease of the output power to 10 mW around 85 °C. At the same time the laser emission wavelength was shifted towards the red, from 1034.5 to 1039 nm, since the laser minimized absorption loss as far as this was advantageous considering the filtering loss from the limited gain bandwidth.

Figure 3.8 shows the pulse duration versus the saturable absorber temperature. We observed stable single-pulse sub-ps mode-locking only around 85 °C in a range of about 10 °C. Here, the pulse had a duration around 300 fs and only very little chirp. For lower temperatures, the pulse broadened, developed a strong tail, became unstable, and the laser switched into a double-, multiple-, or long-pulse regime. This observation can be explained mainly by the decrease of saturable absorption, when tuning the temperature in this direction. Then, passive amplitude modulation became too weak to provide sufficiently strong pulse shaping. The double- or multiple-pulsing tendency was additionally promoted by the increase of the pulse energy due to the lowered loss. Countering this by decreasing the pump power resulted in pulses much longer than those obtained in the optimum range around 85 °C, however. If the SESAM temperature was driven too high, i.e., above 90 °C, the laser switched to a much longer pulse with a center wavelength of ≈1032 nm. This operation regime experienced lower loss from gain filtering, but obviously the contributions to the chirp were not balanced. Although the exact evolution of laser performance with changing SESAM temperature differed somewhat depending on the individual laser configuration and adjustment, so far for all the investigated femtosecond SDLs we observed a similar behavior as in Fig. 3.8.

The optimum SESAM temperatures for shortest-pulse generation obtained from nine experiments (including those from this chapter) are listed in Table 3.1, together with relevant parameters and characteristics of the respective laser configurations. The three saturable absorbers had the same design, but were made for different laser wavelengths. They are distinguished by the center wavelengths of their room temperature photoluminescence (PL) amounting to 1028, 1031 and 1050 nm. The "estimated exciton transition wavelengths" at the operating temperature are based on the room temperature PL, the shift of 10 nm as mentioned above, and a red-shift by about 0.3 nm/°C when increasing the SESAM temperature.

Six gain chips were investigated; chip *A* was a 6-QW structure with ungraded barriers (STIN), chips *B* to *E* were 4-QW graded-barrier designs like in Fig. 3.3b. *F* was a 3-QW graded-barrier design. Compared to the other gain structures, *E* contained no double QW; instead, inhomogeneous broadening was realised by different In-contents in the QWs (designed for a total $\Delta\lambda \approx 6$ nm). *A* to *C* were

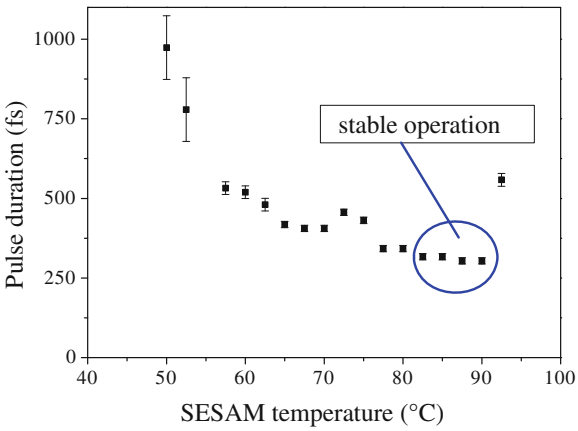


**Fig. 3.8** Pulse duration of the mode-locked SDL measured for different saturable absorber temperatures

2 x 2 $mm^2$ samples (*B* and *C* from the same wafer); *D* to *F* were 4 x 6 $mm^2$ samples. In general, the laser emission wavelength was close to the exciton resonance. The estimation of the exciton transition energy is only rough; we see a trend, however: While in our first experiments, the laser photon energy was rather below the exciton energy, the laser operated energetically at or even slightly above the exciton resonance in the experiments where pulse durations around 200 fs or shorter were obtained. In any case, we observed that heating a SESAM above its optimum operation temperature led to a further decreased output power of the respective SDL and in the shortest-pulse experiments no. 5–9 lasing even ceased above some temperature, which means that effective SESAM absorption was still increasing in this direction.

### *3.4.2 Dependence of Mode-Locked Laser Performance on Pump-Power*

As another important influence for the mode-locked performance we investigated that of the intracavity pulse energy and of the corresponding fluences [22]. In particular, we wanted to know if our SDL would show a behavior typical for soliton-like mode-locking [15, 25].

The pump power incident on the gain medium was varied from 0.77 to 1.32 W, while using an 0.5 % output coupler and keeping the heatsink of the gain chip at 16 °C and that of the SESAM at 106 °C. For the SESAM, the corresponding exciton transition wavelength was estimated at 1047 nm. The laser resonator was 50 mm long.

With femtosecond SDLs, we generally observe two values for the lasing threshold. The lower value is obtained when decreasing the pump power for the already mode-locked laser, since, in this case, the absorber is significantly bleached. When starting the laser, however, the SESAM is practically unbleached; the higher absorption loss will lead to a higher threshold. In this experiment, a pump power of 0.77 W was very close to the laser threshold in case of mode-locking and the lower

limit to permit measurements. Here, the laser would cease emission within less than a minute. When increasing the pump power again, lasing restarted around 1.0 W. The output power showed a linear dependence on the incident pump power, amounting to 4–13 mW around 1045 nm for 0.77–1.24 W of 840-nm pump light. At about 1.32 W of pump radiation, the output power jumped up to 17 mW, indicating that here the onset of ps radiation significantly reduced the total loss of the laser. Probably, spectral hole-burning (SHB) in the gain chip also played a role, because fs pulses can extract only a part of the energy stored in the conduction band, while, for a longer pulse, carriers at higher states within the band become available by intraband relaxation during the course of the pulse.

Figure 3.9 displays a set of nine autocorrelation traces from our SDL. The first trace at the bottom was recorded at 0.77 W of pump power and shows the autocorrelation of a practically perfect $sech^2$ pulse. A $sech^2$ temporal shape is characteristic for optical solitons [15]. The pulse duration did not change much, when the pump power was increased, as can be seen also from Fig. 3.10a presenting the FWHM values obtained from the respective fits. This behavior is not soliton-like. The quality of the fits worsened while increasing the pump power up to 1.00 W. The pulses developed a tail, which was observed as a weak pedestal in the autocorrelation signal. At 1.00 W, single-pulse lasing became unstable. If the laser switched to double pulses at 1.00 W, these were again almost pedestal-free, just like the pulse at 0.77 W. In both cases the output pulse energy was approximately 1.5 pJ, as shown in Fig. 3.10b. If the pump power was increased above 1.00 W, again a pulse tail developed. The related pedestal was most pronounced just before double pulsing became unstable and the laser started producing ps pulses. The ps-pulse shape did not have much to do with $sech^2$ and did not resemble a soliton-like pulse any more.

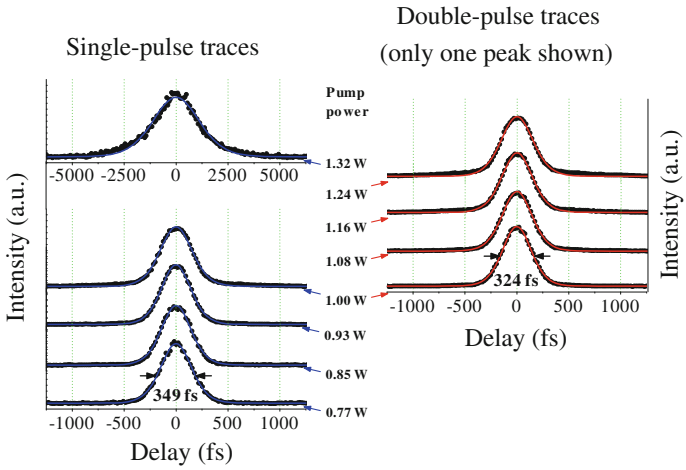


**Fig. 3.9** SDL autocorrelation traces for different pump powers. Respective pump powers are indicated by *arrows*. All traces were background-free; offsets were used to arrange all traces in one graph. *Solid curves* are fits assuming a $sech^2$ pulse shape

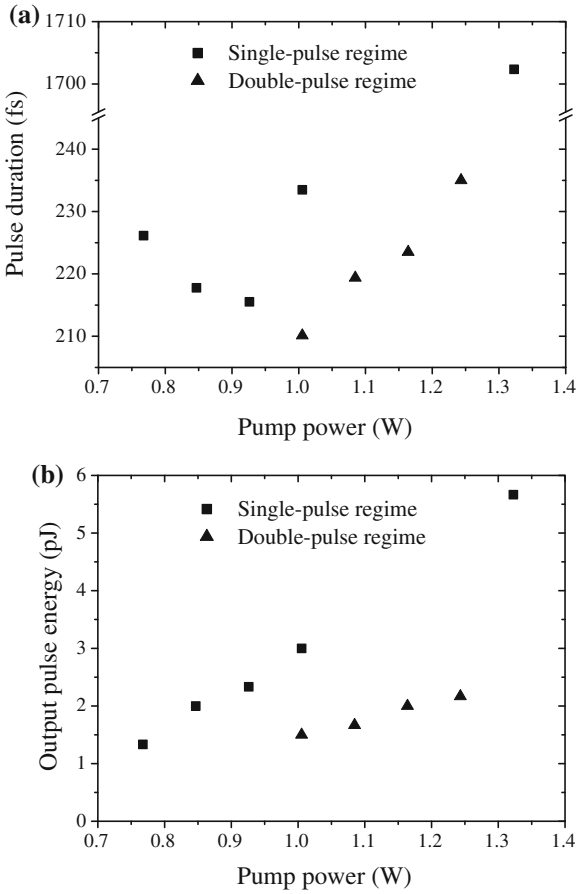


**Fig. 3.10** **a** SDL pulse durations at different pump powers. At 1.00 W there was a transition from single-pulse operation to double pulsing. Slightly above 1.24 W, the laser switched back to single-pulse operation. The pulse duration was much longer, then; please note the axis break. **b** Pulse energies of the mode-locked SDL

Comparing Fig. 3.10a with b illustrates that the pulse durations did not obey the soliton area theorem, which would predict an inverse proportionality of pulse duration and pulse energy [15]. Durations are not even generally shorter for higher energies. Below 1.32 W of pump power, pulses were always around 220 fs. Minimum durations were 215 fs for the single pulse and 210 fs for double pulses. From the highest pulse energy before double pulsing started (Fig. 3.10b), 3 pJ, we estimate a fluence in the order of 100 $\mu J/cm^2$ on the SESAM. This has to be compared to a saturation fluence of 10 $\mu J/cm^2$ we typically determine for our surface-near SESAMs using pulses with similar duration. The onset of double or multiple pulsing in case of an oversaturated absorber is a common phenomenon with soliton-like mode-locking [28]. It is additionally promoted by increased loss from two-photon absorption, which starts to become significant around 100 $\mu J/cm^2$ in the SESAM nonlinear reflectivity curve in Fig. 3.2b, and by SHB in the gain chip. The latter can be explained similarly as for the onset of ps pulses: Carriers at

states not available for a single pulse will relax during the time in between pulses and become available for a second pulse, leading to increased extraction efficiency.

The optical spectra corresponding to the autocorrelation traces in Fig. 3.9 are shown in Fig. 3.11. Only at the respective lowest energies we find single and double pulses to be almost chirp-free, i.e., soliton-like.

For 0.77 W of pump power, we observed emission centered near 1043 nm and a spectral bandwidth (FWHM) of 5.6 nm, corresponding to a time-bandwidth product of 0.35, close to the Fourier limit for a secant hyperbolic. The development of a pulse tail was associated with the coming up of a red shoulder in the spectrum, which extended over almost 10 nm. So, the pulses acquired additional bandwidth, which would be expected for a soliton due to stronger SPM for higher pulse intensity. However, no new frequency components were generated on the blue side with respect to the spectrum at 0.77 W, and the pulse was becoming increasingly chirped.

As the laser switched to double pulses around 1.00 W of pump power, SPM and the saturation of the SESAM were reduced due to lower pulse energy and therefore the largest part of the red shoulder disappeared, growing again with increasing pump power. The evolution of spectral shape and width was very similar for single and double pulses. The shoulder growth was a little faster for the double pulses, if the pulse energies shown in Fig. 3.10b are considered. Picosecond pulses at 1.32 W of pump light corresponded to a spectrum with a FWHM of 1.1 nm.

With increasing pump power, the spectral maximum of the single pulse in Fig. 3.11a was red-shifted from 1043 to 1046 nm; the double-pulse spectral maximum went from 1045 to 1047 nm; the picosecond pulse is centered at 1048 nm. This shift documents the growing heat load. The absorption of the SESAM decreased towards the red; hence, the shift weakened the pulse shaping by the absorber. This resulted in insufficient suppression of the red shoulder and temporal

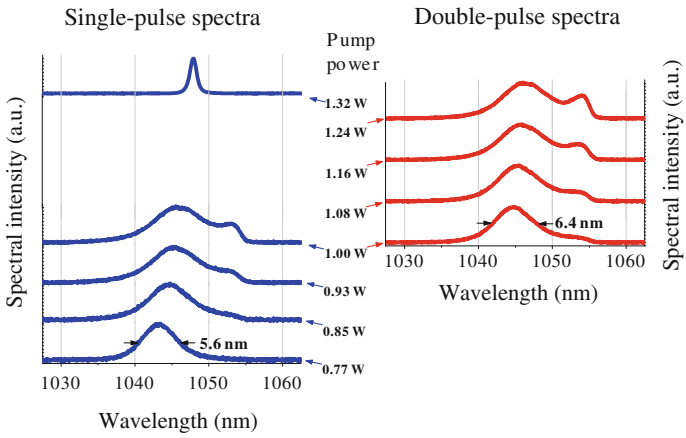


**Fig. 3.11** Optical emission spectra of the mode-locked SDL at different pump powers, recorded simultaneously with the autocorrelation traces shown in Fig. 3.9. Offsets were used to present all spectra in one graph

tail; finally, the bandwidth that is required for sub-ps generation could not be mode-locked any more.

Another way to investigate the influence of the intracavity pulse energy and, hence, of the fluences on the laser performance is by variation of the output coupler transmission $T_{OC}$. Our results with $T_{OC}$ = 0.2–1.5 % (the gain was too low to permit lasing with $T_{OC}$ = 3 %) confirmed our above findings. The minimum pulse durations varied from 190 to 230 fs [22].

### 3.4.3 Discussion—Mode-Locking Mechanism in SDLs

Usually, soliton-like pulse-shaping is required for sub-ps pulse generation in solid state lasers [25]. Some observations typical for soliton-like mode-locking are made with our SDLs as well as with femtosecond lasers using dielectric gain media: temporal shape of intensity close to $sech^2$, practically no chirp for appropriate operation parameters, spectral bandwidth increasing with pulse energy, multiple pulsing at high intracavity powers. However, with our SDLs, there is no inverse proportionality of pulse duration and energy, i.e., the soliton theorem is not fulfilled, and the absorber properties are crucial for SDL pulse durations, while they have little influence on durations in dielectric-media lasers. This indicates, important differences exist with the underlying pulse-shaping effects. Please note, that our sub-ps SDLs are different from the ps SDLs that contain relatively large amounts of intracavity dispersion and that were described as soliton-like in [15, 35].

In lasers based on dielectric gain elements, conditions for very short pulses are a relatively large amount of Kerr SPM, balanced in terms of chirp by appropriate GDD, and minimized spectral filtering effects (particularly, a large gain bandwidth). Passive amplitude modulation (PAM) by an absorber initiates and stabilizes mode-locking, but the absorber modulation depth and relaxation time does not affect the pulse duration much [25].

Pulses in our mode-locked SDL resonator are shaped mainly by the spectro-temporal behavior of saturable absorption and gain and the associated self-phase modulation. Very short pulses can be obtained, if PAM is sufficiently strong, the contributions to chirp largely compensate each other, filtering is minimized, and fast dynamics dominate. This is possible when using a fast SESAM and a broad-gain medium, minimizing GDD, matching SESAM and gain medium, and keeping the laser photon energy close to the excitonic resonance of the SESAM, as shown in Chap. 4 and [22].

If single-pulse operation is desired, too strong saturation of both semiconductor elements must be avoided. However, as SDL pulses become shorter, it is increasingly more difficult to fulfill the latter, since saturation will stem mainly from SHB during the pulse duration and, hence, saturation fluences will be lower than for longer pulses. For pulse durations <200 fs, in our experiments we found stabilization of the single-pulse SDL regime to be a major issue, even if operating close to the lasing threshold. In general, an oversaturated absorber will not suppress

additional pulses in the resonator [28]. We also observed that this inability was more likely or pronounced when we reduced the maximum SESAM modulation depth, lowering the loss handicap for additional pulses this way.

Generally, additional pulses will be promoted by more efficient energy extraction from the gain medium and/or nonlinear losses with inverse saturation characteristics, e.g., two-photon absorption in the SESAM. For lasers with dielectric laser media and soliton-like mode-locking, increased extraction efficiency can be explained by the soliton theorem, i.e., the lower pulse energy in case of multi-pulsing corresponds to a smaller spectral pulse width, which is favourable with respect to the limited spectral bandwidth of the gain. With SDLs, the time constants of the gain chip become important: If the resonator round-trip time is similar to or longer than the recombination time in the gain chip (order of 1 ns), an SDL may produce additional pulses to reduce the amount of laser inversion decaying in between the pulse transits [36]. This will usually lead to a harmonically mode-locked regime. Spatial hole burning, too, will reduce the energy extraction per pulse, if the pulse duration is in the order of or shorter than the carrier-carrier or carrier-phonon scattering times. This was a possible reason why the maximum output pulse energy in Fig. 3.10b was limited to about 3 pJ. The transitions into a femtosecond double-pulse or a picosecond single-pulse regime are motivated by scattering processes that close or avoid the spectral hole in the gain, making more free carriers available for stimulated recombination; energy extraction is more efficient.

We often observed a third, alternative transition when increasing the intracavity pulse intensities, especially the intensity on the gain chip. In this case, multiple pulsing occured not by additional, ungrouped pulses but by emission of pulse groups with close temporal spacings ("macro pulses", "pulse molecules"). These pulse molecules consisted of two to seven pulses. An example is shown in Fig. 3.12 (achieved with gain chip *F*, SESAM "PL at 1031 nm"). Quarterman et al. have found macro pulses with up to 70 peaks [37]. So far, we do not know applications for SDL pulse molecules. Harmonic mode-locking of SDLs enables very high

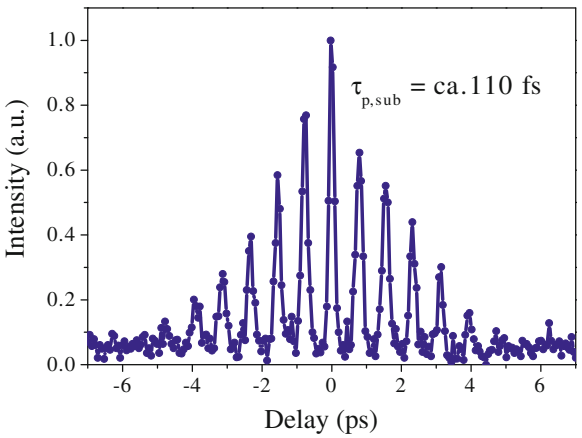


**Fig. 3.12** Autocorrelation trace of a "pulse molecule" containing seven pulses from a mode-locked SDL

repetition rates at sub-picosecond pulse durations, as we will show in the next paragraph. Such a performance is attractive especially for communications with THz data rates via time multiplexing.

## 3.5 High Pulse Repetition Rates and Ultrashort Pulse Durations from a Mode-Locked Semiconductor Disk Laser

### *3.5.1 Sub-200-fs Pulses at 92 GHz Repetition Rate in the Harmonically Mode-Locked Regime*

To obtain short pulses at high repetition rates, we chose a SESAM modulation depth capable of mode-locking a sufficiently broad emission bandwidth and applied a high pump power resulting in a high intracavity power. For this experiment, the four-QW-gain structure labelled *E* in Table 3.1 was used in a ≈29-mm-long "V-shaped" laser cavity. The absorber that matched the gain chip best was the SESAM characterized in Fig. 3.2. Its temperature was stabilized at 20 °C, where the modulation depth amounted to ≈0.6 % at 1030 nm. Taking into account the actual laser wavelength of 1022 nm, we assume a value of about 0.8 % for saturable absorption. Pumping with a power of ≈4 W from an 808-nm laser diode, we detected a trace of separate pulses with a spacing of ≈11 ps. This result is documented by the autocorrelation trace in the 50-ps range in Fig. 3.13a. It corresponds to a repetition rate of ≈92 GHz. This means 18th harmonic-order mode-locking of our laser cavity. The autocorrelation trace recorded in the 1.5-ps range can be approximated assuming a $sech^2$ shape of the pulse intensity and a pulse duration of ≈198 fs (Fig. 3.13b). The 92-GHz rate is confirmed by the optical spectrum (Fig. 3.13c), showing the corresponding modulation with a spacing of approximately 300 pm. Due to the extraordinarily high optical-pulse repetition frequency and bandwidth limitations of photodetectors and microwave analyzers, it was not possible to measure a microwave spectrum of the laser output. For an output coupler transmission of 0.2 %, we measured an output power of 31 mW.

No efforts were made for stabilizing the laser. After several minutes, the spectral comb lost contrast, which could be regained by readjustment of the SDL. In general, with an increasing number of pulses circulating in the cavity, the stability of the laser operation regime will decline. In particular, the number of pulses may vary. Stable harmonic mode-locking with a pulse rate at a demanded value will require an active stabilization of the laser resonator length and the application of a spectral filter (e.g., etalons as sub-cavity) fixing the spectral comb belonging to the desired harmonic order [38]. The filtering approach has already been demonstrated for mode-locked edge emitting laser diodes. Such lasers can reach rates >1 THz without time multiplexing, but one cannot speak of separate pulses. There is a rather sine-shape output due to uncomplete recovery of the saturable absorber and the

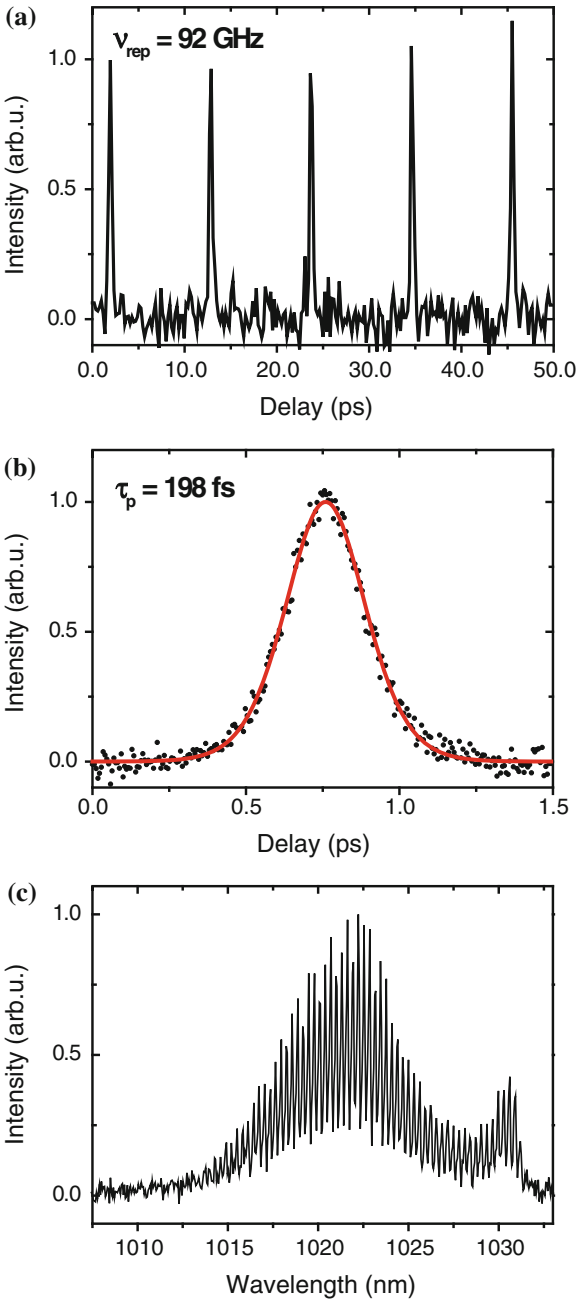


**Fig. 3.13** Harmonically mode-locked semiconductor disk laser at 92 GHz pulse repetition rate:
**a** Autocorrelation trace of the pulse train.
**b** Higher-resolution autocorrelation of one pulse. The fit assuming a $sech^2$ pulse results in a pulse duration $\tau_p$ of 198 fs. **c** Optical spectrum centered near 1022 nm. The mode spacing of ≈300 pm corresponds to the pulse rate $\nu_{rep}$

small number of resonator modes involved in the locking. For SDLs, higher orders of mode-locking and even higher pulse rates than the 92 GHz without multiplexing shown here should be possible, but carrier accumulation in the absorber will turn out as a limitation when the temporal spacing between the pulses becomes too short.

The pulse rate of 92 GHz surpassed the previous 50-GHz rate demonstrated for a mode-locked SDL with 3 ps pulses [24] and, to the best of our knowledge, at present, there is no other laser oscillator—of any kind—combining such a high repetition frequency with a pulse duration below 200 fs. The output power of 31 mW reported here was limited by the available pump power; >100 mW of output should be possible if a higher transmission of the output coupler is chosen (here, $T_{OC}$ was only 0.2 %).

### 3.5.2 107-fs Pulses at 5 GHz Repetition Rate in the Fundamentally Mode-Locked Regime

To achieve a single-pulse regime and the shortest pulses, we increased the SESAM temperature to 68 °C and by this its modulation depth to 1.2 % and reduced the pump power to 2.8 W to keep the pulse intensities moderate on both the SESAM and the gain structure. For the results in Fig. 3.14, we used a 3-QW gain structure (chip *F*). With above 4-QW chip (*E*), minimum pulse durations were 10 fs longer. We estimated fluences of ≈100 μJ/cm$^2$ on the SESAM and ≈6 μJ/cm$^2$ on the gain structure and conclude that, in this SDL, these values were low enough to avoid oversaturation of the semiconductor elements. As shown in Fig. 3.14a, the autocorrelation displayed a pulse duration $\tau_p$ = 107 fs ($sech^2$-shaped intensity assumed). The optical spectrum was centered near 1030 nm and had a full width at half maximum of ≈10.2 nm (Fig. 3.14b). With a time-bandwidth product of ≈0.31, the pulse is approximately Fourier-limited. The small peak near 1046 nm indicates an only weak pulse tail, which is barely visible in the autocorrelation trace. An output power of 3 mW was measured.

The single-pulse regime was documented by a wide-range radio frequency spectrum (Fig. 3.15a), recorded with a 26.5-GHz signal analyzer. The first peak at $\nu_{rep}$ ≈ 5.136 GHz is the fundamental resonance frequency of the laser cavity. Decreased intensities of the higher-order harmonics are due to the limited bandwidth of the photodiode. Figure 3.15b is a higher-resolution scan (5 kHz bandwidth) of the fundamental. The signal-to-noise ratio was ≈70 dB.

In principle, the gain bandwidth of SDLs can support even shorter pulses (see typical PL curve in Fig. 3.4). In [37], with an SDL, pulse bunches were observed, which had an envelope of a few ps and revealed a substructure of ≈60-fs peaks. However, no single-pulse operation was achieved, which was explained by the influence of SHB in the gain chip. Therefore, to the best of our knowledge, the 107-fs pulses set a new milestone for pulse durations from fundamentally mode-locked

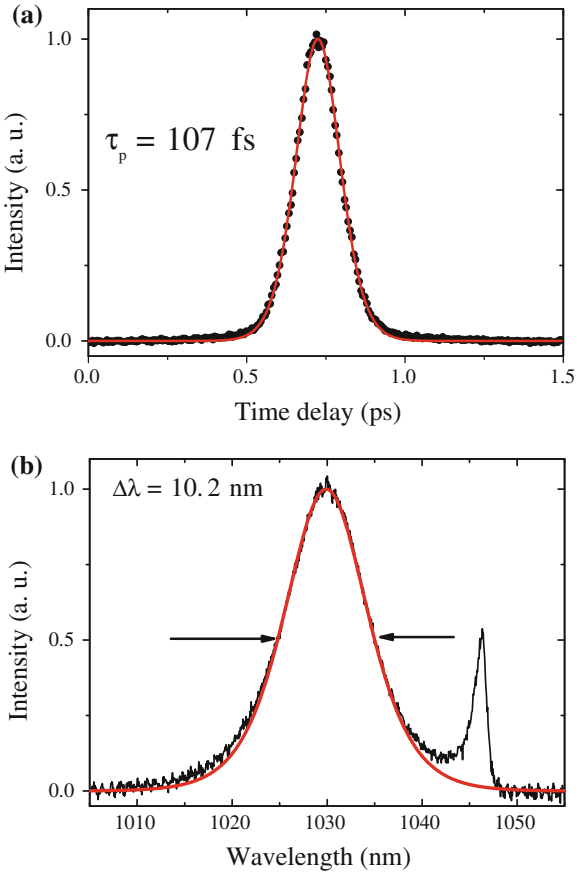


**Fig. 3.14** **a** Autocorrelation trace of the semiconductor disk laser in the single-pulse regime. A $sech^2$ fit yields a pulse duration $\tau_p$ of 107 fs. **b** Optical spectrum centered near 1030 nm

SDLs (and from any fundamentally or harmonically mode-locked semiconductor laser without external pulse compression). The result shows that SHB does not prevent single-pulse operation of SDLs at ultrashort pulse durations. Nevertheless, SHB must be considered a severe issue when trying to achieve high output powers and high pulse energies with single-pulse operation and pulse durations in the 100-fs range at the same time. While power scaling is relatively easy for cw or picosecond SDLs, the average output power of 120 mW for a pulse duration of 355 fs at 1 GHz in [39] is the highest reported so far for sub-500 fs SDLs. Moderate improvement of the value of 3 mW demonstrated here with $T_{OC}$ = 0.2 % can be expected with a higher output coupler transmission. However, operating the SDL much further above the lasing threshold will drive the laser into multiple-pulsing.

A way to boost the ultrashort-pulse output of SDLs to power levels required for applications is by use of tapered diode amplifiers (TDAs) and/or fiber amplifiers [22, 40]. A TDA with pulsed electrical pumping is capable of acting both as an amplifier and as a fast pulse picker. This approach will give free choice of pulse repetition frequency and make SDL systems applicable also for uses requiring

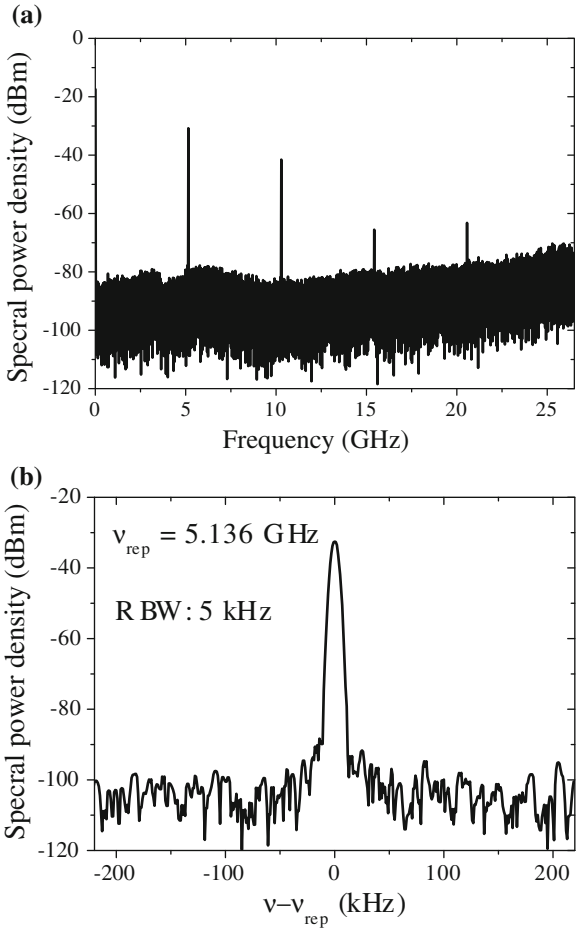


**Fig. 3.15** Radio frequency spectrum of the SDL in the single-pulse regime. **a** Wide range spectrum. The fundamental laser frequency is $\nu_{rep} \approx 5.136$ GHz. **b** Vicinity of the fundamental mode

lower repetition frequencies. As a proof of principle, in [22], we examined a TDA/SDL combination and reduced the pulse repetition frequency from 3 GHz to 47 MHz.

## 3.6 Summary

This chapter addressed the generation of femtosecond pulses with passively mode-locked semiconductor disk lasers (SDLs) in the 1-μm wavelength range. We investigated the optimum parameters for almost chirp-free femtosecond pulses in single- or multiple-pulse regimes. On the whole, the pulse-shaping process in our SDLs is not "soliton-like" in the classical picture applied to dielectric-gain-media lasers. In particular, the pulse durations strongly depended on the relaxation behavior

and the effective modulation depth of the semiconductor saturable absorber mirror (SESAM). Throughout, we used semiconductor media with minimized group delay dispersion, i.e., with antireflective coatings and thin active zones. Wavelength matching of gain chip and SESAM was essential for ultrashort-pulse generation, achieving a sufficiently deep absorber modulation. Spectral-hole burning (SHB) of both gain chip and absorber affected the stability of single-pulse operation. For fundamental mode-locking, operation close to the lasing threshold was required, avoiding too strong saturation of the semiconductor elements.

Based on our findings, we built a harmonically mode-locked SDL emitting 198-fs pulses at a very high repetition rate of ≈92 GHz and a fundamentally mode-locked SDL demonstrating 107-fs pulses at a rate of ≈5 GHz. The 92-GHz result should fuel interest in using SDLs for communications or frequency comb generation. At present, there seem to be no other laser oscillators that can generate sub-200-fs pulses at such high rates. The practically chirpfree 107-fs pulses shown here set a new record for shortest pulse durations achieved directly from any fundamentally or harmonically mode-locked semiconductor laser. With respect to pulse durations for mode-locked lasers in this emission region, InGaAs/(Al)GaAs SDL gain media now surpass typical $Nd^{3+}$-doped crystals and compete with $Yb^{3+}$-doped media. Combination of SDLs with electrically pumped tapered diode amplifiers offers an elegant approach to boost the output power and to realize variable pulse repetition rates (in principle, down to 1 Hz) [22].

Overall, the results are a further step of mode-locked SDLs in becoming useful compact and low-cost ultrashort-pulse sources. They are especially attractive for applications requiring high pulse repetition rates, like in THz spectroscopy [3]. In principle, following the same strategies with other semiconductor material systems, similar results should be obtainable in other spectral regions.

## References

1. H. Yoshida, Y. Yamashita, M. Kuwabara, H. Kan, A 342-nm ultraviolet AlGaN multiple-quantum-well laser diode. Nat. Photonics **2**, 551–554 (2008)
2. K.J. Linden, Single mode, short cavity, Pb-salt diode lasers operating in the 5, 10, and 30 μm spectral regions. IEEE J. Quantum Electron. **21**, 391–394 (1985)
3. R. Gebs, P. Klopp, G. Klatt, T. Dekorsy, U. Griebner, A. Bartels, Time-domain THz spectroscopy based on asynchronous optical sampling with a femtosecond semiconductor disk laser. Electron. Lett. **46**, 75 (2010)
4. F. Quinlan, G. Ycas, S. Osterman, S.A. Diddams, A 12.5 GHz-spaced optical frequency comb spanning > 400 nm for near-infrared astronomical spectrograph calibration. Rev. Sci. Instr. **81**, 063105 (2010)
5. U. Keller, A.C. Tropper, Passively modelocked surface-emitting semiconductor lasers. Phys. Rep. **429**, 67–120 (2006)
6. S.L. Chuang, *Optoelectronic Devices* (Wiley, New York, 1995)
7. C.W. Wilmsen, H. Temkin, L.A. Coldren (eds.), *Vertical-Cavity Surface-Emitting Lasers: Design, Fabrication, Characterization, and Applications* (Cambridge University Press, Cambridge, 1999)

8. M. Kuznetsov, F. Hakimi, R. Sprague, A. Mooradian, Design and characteristics of high-power (>0.5-W CW) diode-pumped vertical-external-cavity surface-emitting semiconductor lasers with circular TEM00 beams. IEEE J. Sel. Top. Quantum Electron. **5**, 561–573 (1999)
9. C. Steven, K. Contag, M. Larionov, A. Giesen, H. Hügel, A 1-kW CW thin disk laser. J. Sel. Top. Quantum Electron. **6**, 650–657 (2000)
10. J.L. Chilla, S.D. Butterworth, A. Zeitschel, J.P. Charles, A.L. Caprara, M.K. Reed, L. Spinelli, in *High power optically pumped semiconductor lasers,* ed. by R. Scheps, H.J. Hoffman. Solid State Lasers XIII: Technology and Devices. Proc. SPIE **5332**, 143–150 (2004)
11. B. Rudin, A. Rutz, M. Hoffmann, D.J.H.C. Maas, A.-R. Bellancourt, E. Gini, T. Südmeyer, U. Keller, Highly efficient optically pumped vertical-emitting semiconductor laser with more than 20 W average output power in a fundamental transverse mode. Opt. Lett. **33**, 2719–2721 (2008)
12. C. Hönninger, R. Paschotta, F. Morier-Genoud, M. Moser, U. Keller, Q-switching stability limits of continuous-wave passive mode locking. J. Opt. Soc. Am. B **16**, 46–56 (1999)
13. M.E. Barnes, Z. Mihoubi, K.G. Wilcox, A.H. Quarterman, I. Farrer, D.A. Ritchie, A. Garnache, S. Hoogland, V. Apostolopoulos, A.C. Tropper, Gain bandwidth characterization of surface-emitting quantum well laser gain structures for femtosecond operation. Opt. Express **18**, 21330–21341 (2010)
14. S. Hoogland, S. Dhanjal, A.C. Tropper, J.S. Roberts, R. Häring, R. Paschotta, F. Morier-Genoud, U. Keller, Passively mode-locked diode-pumped surface-emitting semiconductor laser. IEEE Photon. Technol. Lett. **12**, 1135–1137 (2000)
15. R. Paschotta, R. Häring, A. Garnache, S. Hoogland, A.C. Tropper, U. Keller, Soliton-like pulseshaping mechanism in passively mode-locked surface-emitting semiconductor lasers. Appl. Phys. B **75**, 445–451 (2002)
16. A. Garnache, S. Hoogland, A.C. Tropper, I. Sagnes, G. Saint-Girons, J.S. Roberts, Sub-500-fs soliton-like pulse in a passively mode-locked broadband surface-emitting laser with 100 mW average power. Appl. Phys. Lett. **80**, 3892–3894 (2002)
17. S. Hoogland, A. Garnache, I. Sagnes, J.S. Roberts, A.C. Tropper, 10-GHz Train of Sub-500-fs optical soliton-like pulses from a surface-emitting semiconductor laser. IEEE Photon. Technol. Lett. **17**, 267–269 (2005)
18. S. Arahira, S. Oshiba, Y. Matsui, T. Kunii, Y. Ogawa, Terahertz-rate optical pulse generation from a passively mode-locked semiconductor laser diode. Opt. Lett. **19**, 834–836 (1994)
19. E.U. Rafailov, M.A. Cataluna, W. Sibbett, N.D. Il'inskaya, Yu. M. Zadiranov, A.E. Zhukov, V.M. Ustinov, D.A. Livshits, A.R. Kovsh, N.N. Ledentsov, High-power picosecond and femtosecond pulse generation from a two-section mode-locked quantum-dot laser. Appl. Phys. Lett. **87**, 081107 (2005)
20. P. Klopp, F. Saas, M. Zorn, M. Weyers, U. Griebner, 290-fs pulses from a semiconductor disk laser. Opt. Express **16**, 5770–5775 (2008)
21. K.G. Wilcox, Z. Mihoubi, G.J. Daniell, S. Elsmere, A. Quarterman, I. Farrer, D.A. Ritchie, A. Tropper, Ultrafast optical Stark mode-locked semiconductor laser. Opt. Lett. **33**, 2797 (2008)
22. P. Klopp, U. Griebner, M. Zorn, A. Klehr, A. Liero, M. Weyers, G. Erbert, Mode-locked InGaAs-AlGaAs disk laser generating sub-200-fs pulses, pulse picking and amplification by a tapered diode amplifier. Opt. Express **17**, 10820 (2009)
23. P. Klopp, U. Griebner, M. Zorn, M. Weyers, Pulse repetition rate up to 92 GHz or pulse duration shorter than 110 fs from a mode-locked semiconductor disk laser. Appl. Phys. Lett. **98**, 071103 (2011)
24. D. Lorenser, J.H.C. Maas, H.J. Unold, A.-R. Bellancourt, B. Rudin, E. Gini, D. Ebeling, U. Keller, 50-GHz passively mode-locked surface-emitting semiconductor laser with 100-mW average output power. IEEE J. Quantum Electron. **42**, 838–847 (2006)
25. F.X. Kärtner, I.D. Jung, U. Keller, Soliton mode-locking with saturable absorbers. IEEE J. Selected Topics Quantum Electron. **2**, 540–556 (1996)
26. U. Zeimer, J. Grenzer, D. Korn, S. Döring, M. Zorn, W. Pittroff, U. Pietsch, F. Saas, M. Weyers, X-ray diffraction spot mapping—a tool to study structural properties of semiconductor disk laser devices. Phys. Stat. Sol. (a) **204**, 2753–2759 (2007)

27. F. Saas, G. Steinmeyer, U. Griebner, M. Zorn, M. Weyers, Exciton resonance tuning for the generation of sub-picosecond pulses from a mode-locked semiconductor disk laser. Appl. Phys. Lett. **89**, 141107 (2006)
28. M.J. Lederer, B. Luther-Davies, H.H. Tan, C. Jagadish, N.N. Akhmediev, J.M. Soto-Crespo, Multipulse operation of a Ti:sapphire laser mode locked by an ion-implanted semiconductor saturable-absorber mirror. J. Opt. Soc. Am. B **16**, 895–904 (1999)
29. J.W. Tomm, V. Strelchuk, A. Gerhardt, U. Zeimer, M. Zorn, H. Kissel, M. Weyers, J. Jimenez, Properties of $As^{+}$-implanted and annealed GaAs and InGaAs quantum wells: Structural and band-structure modifications. J. Appl. Phys. **95**, 1122–1126 (2004)
30. M. Zorn, P. Klopp, F. Saas, A. Ginolas, O. Krüger, U. Griebner, M. Weyers, Semiconductor components for femtosecond semiconductor disk lasers grown by MOVPE. J. Crystal Growth **310**, 5187–5190 (2008)
31. M. Haiml, R. Grange, U. Keller, Optical characterization of semiconductor saturable absorbers. Appl. Phys. B **79**, 331–339 (2004)
32. F. Saas, V. Talalaev, U. Griebner, J.W. Tomm, M. Zorn, A. Knigge, M. Weyers, Optically pumped semiconductor disk laser with graded and step indices. Appl. Phys. Lett. **89**, 151120 (2006)
33. M. Moenster, U. Griebner, W. Richter, G. Steinmeyer, Resonant saturable absorber mirrors for dispersion control in ultrafast lasers. IEEE J. Quantum Electron. **43**, 174–181 (2007)
34. P. Klopp, F. Saas, U. Griebner M. Zorn, M. Weyers, Passively mode-locked semiconductor disk laser generating sub-300-fs pulses. CLEO/QELS 2008, CThF6
35. M. Hoffmann, O.D. Sieber, D.J.H.C. Maas, V.J. Wittwer, M. Golling, T. Südmeyer, U. Keller, Experimental verification of soliton-like pulseshaping mechanisms in passively mode-locked VECSELs. Opt. Express **18**, 10143–10153 (2010)
36. E.J. Saarinen, R. Herda, O.G. Okhotnikov, Dynamics of pulse formation in mode-locked semiconductor disk lasers. J. Opt. Soc. Am. B **24**, 2784–2790 (2007)
37. A.H. Quarterman, K.G. Wilcox, V. Apostolopoulos, Z. Mihoubi, S.P. Elsmere, I. Farrer, D.A. Ritchie, A. Tropper, A passively mode-locked external-cavity semiconductor laser emitting 60-fs pulses. Nat. Photonics **3**, 729 (2009)
38. S. Arahira. S. Oshiba, Y. Matsui, T. Kunii, Y. Ogawa, 500 GHz optical short pulse generation from a monolithic passively mode-locked distributed Bragg reflector laser. Appl. Phys. Lett. **64**, 1917–1919 (1994)
39. K.G. Wilcox, A.H. Quarterman, H. Beere, D.A. Ritchie, A.C. Tropper, High peak power femtosecond pulse passively mode-locked vertical-external-cavity surface-emitting laser. IEEE Photon. Technol. Lett. **22**, 1021–1023 (2010)
40. P. Dupriez, C. Finot, A. Malinowski, J.K. Sahu, J. Nilsson, D.J. Richardson, K.G. Wilcox, H. D. Foreman, A.C. Tropper, High-power, high repetition rate picosecond and femtosecond sources based on Yb-doped fiber amplification of VECSELs. Opt. Express **14**, 9611–9616 (2006)